High-resolution spectroscopy of the 1*S*-2*S* transition in atomic hydrogen

A. Huber, B. Gross, M. Weitz, and T. W. Hänsch
Max-Planck-Institut für Quantenoptik, Hans-Kopfermann-Strasse 1, 85748 Garching, Germany
(Received 27 July 1998)

The sharp hydrogen 1*S*-2*S* two-photon transition is a promising candidate for the realization of a frequency standard based on an atomic transition in the optical region. In recent work we have used this transition to precisely determine the Rydberg constant, the 1*S* Lamb shift and the hydrogen-deuterium isotope shift. In this paper we focus on substantially improved spectroscopic methods leading to a much higher spectral resolution of the 1*S*-2*S* transition in hydrogen and deuterium. We have successfully applied a time-delayed measurement scheme, which allowed us to reduce the linewidth to 1 kHz at 243 nm corresponding to a spectral resolution of $\Delta\nu/\nu=8\times10^{-13}$. A theoretical line-shape model based on a solution of the Master equation allows us to determine the unperturbed hydrogen 1*S*-2*S* two-photon transition frequency from our spectra to a level of 1.5×10^{-14}. [S1050-2947(99)06202-2]

PACS number(s): 32.30.Jc, 42.62.Fi, 06.20.Jr, 07.60.Rd

I. INTRODUCTION

The hydrogen atom has played a central role in the development of fundamental laws of physics. The Doppler-free 1*S*-2*S* two-photon transition with a natural linewidth of 1.3 Hz offers a challenging potential for precision measurements. Based on this transition, measurements of the Rydberg constant, the most precisely known constant in physics, and of the 1*S* Lamb shift have been performed [1–3]. The experimentally determined value of the 1*S* Lamb shift is currently the most stringent test of the theory of quantum electrodynamics (QED) in an atom. Further, from the difference of the 1*S*-2*S* frequency in hydrogen and deuterium the structure radius of the deuteron, an important quantity of nuclear physics, has been derived with unrivaled accuracy [4]. Moreover, two-photon spectroscopy of the 1*S*-2*S* transition has proved to be a valuable tool in the recent successful study of Bose-Einstein condensation of magnetically trapped atomic hydrogen [5].

Here we report on recent advances concerning the spectral resolution of the 1*S*-2*S* transition, which is recommended for the future realization of an atomic clock in the optical region [6]. By refined spectroscopic methods in combination with elaborate theoretical calculations, we can determine the unperturbed hydrogen 1*S*-2*S* two-photon transition frequency from our spectra to a level of 1.5×10^{-14}. This paper describes in detail the theoretical model used to analyze the experimental hydrogen spectra.

II. THE HYDROGEN 1*S*-2*S* SPECTROMETER

Figure 1 shows the spectrometer we use to excite the $1S_{1/2}(F=1,m_F=\pm1)-2S_{1/2}(F=1,m_F=\pm1)$ transition in hydrogen. This Doppler-free two-photon transition is driven in a cold atomic beam with the frequency doubled radiation of an ultrastable dye laser at 486 nm. The resulting UV radiation at 243 nm is resonantly enhanced in a linear cavity inside a vacuum chamber. A detailed description of the laser system is given in Ref. [7]. A liquid-helium-cooled nozzle forms a beam of hydrogen atoms produced by dissociation of molecules in a gas discharge. The beam is traveling collinearly to the UV standing wave. At a distance of $d\simeq13$ cm from the nozzle the fraction of atoms that have been excited to the metastable 2*S* state is probed by an electric quenching field forcing the emission of Lyman-α photons, which can be detected by a solar-blind photomultiplier tube. A chopper periodically blocks the 243-nm UV light. The photomultiplier is read out only in the periods with blocked UV light to avoid background counts. A delay time τ between blocking the laser light and registering the signal of excited atoms selects the signal of slow atoms with velocities v less than $v_{max}=d/\tau$. By using only slow atoms to contribute to the signal, the two main systematic effects that both depend on the atomic velocity, i.e., time-of-flight broadening and the second-order Doppler shift, are substantially reduced. With the help of a multichannel photon counter we register all signal photons as function of their arrival time in a set of discrete steps τ_i. This allows us to reconstruct the signal corresponding to different delay times by adding up all signal photons that arrived with a delay time of $\tau>\tau_i$ after the light was blocked. A time-delayed spectrum, consisting of seven single spectra simultaneously recorded, is shown in Fig. 2. The temperature of the nozzle was 70.2 K.

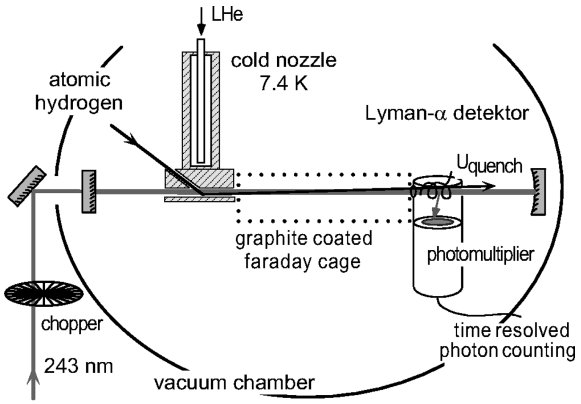

FIG. 1. Experimental setup for the excitation of the 1*S*-2*S* two-photon transition in a cold beam of atomic hydrogen, oriented collinearly to a standing wave of UV light at 243 nm inside an enhancement resonator.

 ©1999 The American Physical Society

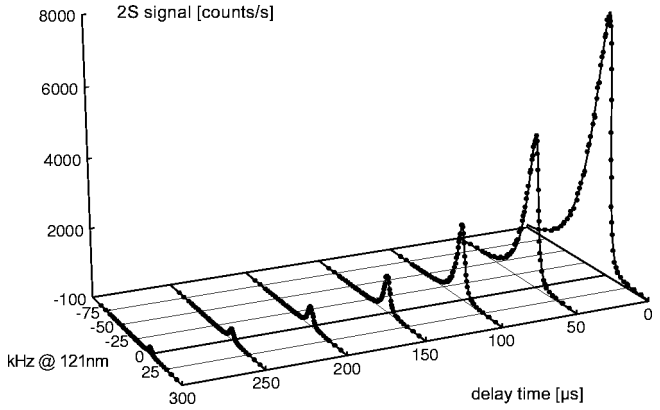

FIG. 2. Time-resolved $1S$-$2S$ spectrum in atomic hydrogen, recorded at a nozzle temperature of 70.2 K. The solid line is a fit to the experimental data using the line-shape model presented below.

In this spectrum the reduction of the linewidth with increasing delay time is clearly visible. More importantly, the shift due to second-order Doppler effect also decreases significantly with higher delay times.

While the spectrum recorded at 70.2 K is presented mainly for illustration purposes, a higher resolution is obtained when the nozzle temperature is lowered to 7 K. Figure 3 illustrates how the maximum velocity depends on the chosen delay time. Due to the selection of atoms from the slow tail of the velocity distribution, the amplitude of the observed signal is reduced for increasing delay times. Nevertheless, with the method of time-delayed signal detection we have observed hydrogen $1S$-$2S$ spectra with linewidths down to 1 kHz at 243 nm, corresponding to a spectral resolution of $\Delta\nu/\nu = 8\times10^{-13}$, as shown in Fig. 4. For this figure two scans have been averaged leading to a total measurement time of 2 s per point. The temperature of the nozzle is 7.4 K and the delay time 1600 μs. Only atoms with velocities less than 80 m/s contribute to the signal, resulting in an upper limit for the second-order Doppler shift of only 44 Hz at 121 nm.

III. THEORETICAL LINE-SHAPE MODEL

In this section we present a line-shape model worked out to compare the time-resolved experimental spectra to theoretical predictions. Fitting of the calculated data to the experimental spectra allows the determination of the unperturbed $1S$-$2S$ transition frequency from the experimental spectra to high accuracy.

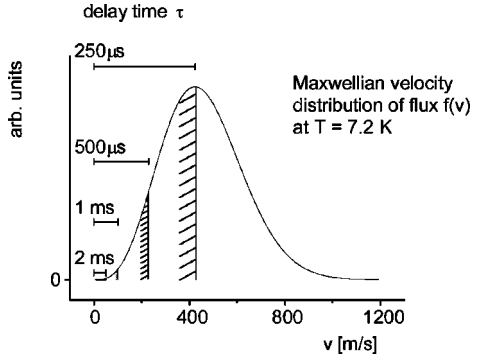

FIG. 3. Selection of slow atoms. The higher the delay time τ, the smaller the maximum velocity v_{max} of an atom that can contribute to the $2S$ signal.

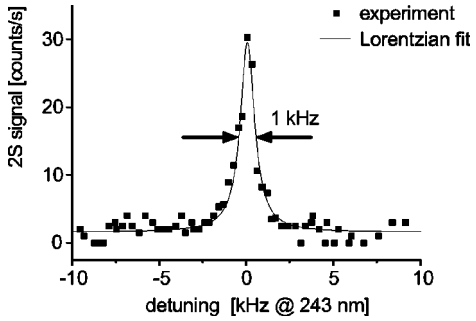

FIG. 4. Time-delayed hydrogen $1S$-$2S$ spectrum with a linewidth of 1 kHz at 243 nm, recorded at a nozzle temperature of 7.4 K.

Our calculations are based on a description of the hydrogen atom as a quantum mechanical two-level system in a density matrix formalism [8–10]. We chose the representation of the density operator in the basis of energy eigenstates. The time evolution of the density matrix ρ obeys the Master equation:

$$\dot{\rho} = \frac{1}{i\hbar}[\mathbf{H},\rho] + \dot{\rho}_{relax}, \tag{1}$$

with

$$\rho = \begin{bmatrix} \rho_{aa} & \rho_{ab} \\ \rho_{ba} & \rho_{bb} \end{bmatrix} \tag{2}$$

and

$$\mathbf{H} = \mathbf{H}_0 + \mathbf{H}' = \begin{bmatrix} \hbar\omega_a & 0 \\ 0 & \hbar\omega_b \end{bmatrix} + \begin{bmatrix} 0 & H^*_{ab} \\ H^*_{ba} & 0 \end{bmatrix}. \tag{3}$$

Here, the diagonal elements ρ_{aa} and ρ_{bb} stand for the population of the $1S_{1/2}(F=1)$ ground state and $2S_{1/2}(F=1)$ excited state, respectively. The off-diagonal elements describe the coherence between both states induced by the action of the driving light field where $\rho_{ba} = \rho^*_{ab}$ since ρ is Hermitian. The unperturbed atomic Hamiltonian is denoted as $\mathbf{H}_0$. The interaction operator $\mathbf{H}'$ acts on the time evolution of the density matrix and leads to a population transfer. Relaxation processes such as spontaneous decay are described by $\dot{\rho}_{relax}$. Here, in a good approximation, we can set $\dot{\rho}_{relax} = 0$, since the lifetime of the metastable $2S$ state is about 1/7 s, being much larger than our experimentally possible interaction time. For H^*_{ab}, we write in the case of two-photon excitation,

$$H^*_{ab} = M_{ab}\left(\frac{\vec{E}_0}{2}(e^{i\omega_L t} + e^{-i\omega_L t})\right)^2$$
$$= M'_{ab} I_L (e^{i2\omega_L t} + e^{-i2\omega_L t} + 2). \tag{4}$$

In this formula I_L denotes the intensity and ω_L the frequency of the excitation light field. We use $\vec{E}_0^2 = 2I_L/c\ \epsilon_0$. The matrix element is $M_{ab} = \gamma e^2 a_0^2/\alpha^2 mc^2$ with $\gamma = 7.85$ for the

$1S$-$2S$ two-photon transition in hydrogen (atomic units) [11]. From this one derives the value $M'_{ab}=2.4398\times10^{-38}$ J $(\mathrm{W/m^2})^{-1}$. In the next step we separate the slow time evolution ρ'_{ij} from the density matrix elements that oscillate at optical frequencies:

$$\rho_{ij}=\rho'_{ij}e^{i2\omega_L t}. \tag{5}$$

Taking all previous definitions together and performing the rotating wave approximation we obtain a set of coupled differential equations describing the atom in the laboratory frame:

$$\dot{\rho}'_{aa}(t)=-\frac{2}{\hbar}M'_{ab}I_L\mathrm{Im}[\rho'_{ab}(t)],$$

$$\dot{\rho}'_{bb}(t)=\frac{2}{\hbar}M'_{ab}I_L\mathrm{Im}[\rho'_{ab}(t)], \tag{6}$$

$$\dot{\rho}'_{ab}(t)=-i\Delta\omega\rho'_{ab}(t)-\frac{i}{\hbar}M'_{ab}I_L[\rho'_{bb}(t)-\rho'_{aa}(t)].$$

Here $\Delta\omega=2\omega_L-\omega_{ba}$ denotes the laser detuning from the atomic resonance frequency ω_{ba}. For fixed values of $\Delta\omega$ and I_L the above system of equations describe the well-known Rabi oscillations. For small t and weak fields the upper state population $\rho'_{bb}(t)$ grows quadratically in time assuming $\rho'_{bb}(t=0)=0$. With this system of coupled differential equations we can calculate the theoretical line shape of the $1S$-$2S$ transition for our excitation geometry. We assume that an atom with velocity v follows a classical trajectory through the standing wave laser field starting in the nozzle and ending in the detector. While at the beginning of a trajectory ($t=0$), the atom is in the $1S$ ground state, the interaction with the light field transfers population to the excited state given by $\rho'_{bb}(t)$. This occupation is probed at time T_f in the $2S$ detector. Here, we assume that T_f is the time when the atom reaches the center of the detector, not taking into account the actual spatial dependence of the quenching field that mixes the metastable $2S$ state with the rapidly decaying $2P$ state. We model the light field as a standing wave of frequency ω_L with a Gaussian beam profile given by the geometry of our enhancement resonator [12]. To switch from the laboratory to the atomic frame we replace I_L by $I_L(r(t),z(t))$, where $r(t)$ denotes the radial distance from the beam center and $z(t)$ is the distance from the nozzle. These two parameters suffice to characterize the instantaneous light intensity experienced by the atom during the flight through the standing wave.

The relativistic Doppler shift is taken into account by replacing the laser frequency $2\omega_L$ by $2\omega_L[1+\frac{1}{2}(v/c)^2]$. The detuning can now be expressed as

$$\Delta\omega=2\omega_L-\omega_{ba}+\left(\frac{v}{c}\right)^2\omega_L. \tag{7}$$

We describe the switching of the light field by the mechanical chopper simply by multiplying the light intensity I_L with a periodic step function $R(t)$, which takes the values zero and one corresponding to light blocked and not blocked, respectively. We assume an instantaneous switching with infinitely steep slope. In the experiment, the chopper frequency is set to values between 160 Hz and 500 Hz. We define the chopper phase ϕ_{ch} as the phase difference between the time when an atom starts from the nozzle and the next jump of $R(t)$ from the value zero to unity. The contribution of an atom reaching the $2S$ detector can now be written as

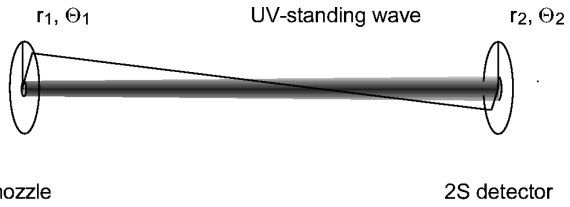

FIG. 5. Example of an atomic trajectory through the excitation light field. The radii of the nozzle and the aperture in front of the $2S$ detector are 0.5 and 1.05 mm, respectively. The distance d between nozzle and detector is 133 mm.

$$\rho'_{bb}(T_f)_{\Delta\omega}=\rho'_{bb}\left(T_f=\frac{d}{v},\vec{r_1},\vec{r_2},\phi_{ch}\right)_{\Delta\omega}. \tag{8}$$

Here d denotes the distance between the nozzle and the detector. $\vec{r_1}=(r_1,\theta_1)$ and $\vec{r_2}=(r_2,\theta_2)$ give the coordinates of the start and end point of the trajectory in which the atom is moving with velocity v. From these parameters the laser intensity $I_L(r(t),z(t))$ as illustrated in Fig. 5 is easily calculated. We assume that all starting points of atomic trajectories are in the nozzle orifice plane. For a calculation of $\rho'_{bb}(T_f)_{\Delta\omega}$ we solve the system of coupled differential equations (6) numerically with the fourth-order Runge-Kutta algorithm [13]. To account for the experimental situation we have to integrate over all possible trajectories, the velocity distribution, and the chopper phase. A calculated spectrum is obtained by evaluating the following expression for a set of different detunings:

$$S(\Delta\omega)=\int_v f(v)\,dv\int\int\int\int_{space}d\vec{r_1}\,d\vec{r_2}\int_{chopper}d\phi_{ch}$$
$$\times\rho'_{bb}\left(t=T_f=\frac{d}{v},\vec{r_1},\vec{r_2},\phi_{ch}\right)_{\Delta\omega}. \tag{9}$$

The four-dimensional integral over the nozzle and detector apertures can be reduced to three dimensions by symmetry considerations. Nevertheless, including the time integration, this is a six-dimensional expression, which has to be solved for a set of detunings $\Delta\omega$. Altogether the entire solution is extremely time consuming when evaluated numerically. An efficient program code has been developed such that the problem could be solved with a convergence of the line center at a level of 0.1% of the linewidth.

Up to now, no assumptions have been made concerning the velocity distribution $f(v)$, which critically affects the dominant systematic effects, namely, time-of-flight broadening and second-order Doppler shift. At this point, our approach differs from that used in [7]. Since the temperature of the nozzle can be varied, significantly changing the velocity distribution, we want to circumvent the need for solving the equations again and again for every different temperature.

For that reason and the fact that the shape of the velocity distribution is not known exactly, we decided to determine the characteristic parameters of the velocity distribution during a fit of the calculated data to the experimental spectra. We have calculated the expression given in Eq. (9) for discrete velocities v_j and discrete detunings, and arranged the results in a matrix m_{ij} where i specifies the laser detuning and j the atomic velocity. With these numbers an integration over the velocity distribution can be done subsequently during data analysis. The velocities v_j are such as to allow integration via the Gauss-Legendre method. In fact, by this approach we calculate a set of typically 40 matrices, each matrix belonging to a certain delay time in the sense of the time-delayed measurement technique. To fit the theoretical data to the experimental spectra we prepare the experimental spectra as follows. Since the spectra shown in this paper have been recorded with the laser locked to an external reference cavity that slowly drifts in time, we first compensate this drift. The maximum signal recorded in each single scan can serve as an absolute frequency marker that is used to approximate the drift rate. For this procedure we usually use the signal with a delay time of 800 μs. The compensation of the drift is necessary for a subsequent averaging over several scans. For further data analysis we only use data points that have been recorded under similar conditions as far as the nozzle temperature, the pressure in the vacuum chamber, and the UV power of the excitation light field are concerned. Then, in a second step, the signals with different delay times are rescaled to a uniform amplitude to ensure that all spectra are statistically equally represented during the simultaneous fit with the Levenberg-Marquart algorithm, which is performed with spline interpolated values of the line-shape model similar to the appoach in [14]. After a successful fit, the amplitudes are scaled back in a third step.

For an atomic beam formed by a nozzle as in our experiment, a Maxwellian velocity distribution is expected for the flux of atoms at the $2S$ detector [15]:

$$f(v)=\frac{1}{N}v^3 e^{-(v/v_0)^2} \tag{10}$$

with

$$v_0=\sqrt{2kT/M}. \tag{11}$$

Here, v is the atomic velocity, v_0 the most probable velocity, k the Boltzmann constant, M the atomic mass, T the temperature of the atomic beam, and N a normalization factor. The approximation $v=\sqrt{v_x^2+v_y^2+v_z^2}\sim v_z$ is made since the apertures select only atoms with $v_z \geqslant 85|v_{x,y}|$. This velocity distribution of the flux can be used to fit the theoretical data to the experimental spectra. The minimum number of fit parameters is three: one universal amplitude A valid for all spectra with different delay times, the most probable velocity v_0, from which the corresponding temperature T can be easily derived, and a quantity Δ_{det} to adjust the frequency axes of the theoretical and experimental data with respect to each other. The fitted value of Δ_{det} permits correcting the transition frequency for the second-order Doppler shift. The temperature corresponding to the fitted value of v_0 is a measure of how well the atomic beam is thermalized with the walls of the nozzle. From the amplitude A, in principle, the number of hydrogen atoms in the atomic beam can be determined. It turns out that with only these three fit parameters, it is not possible to model the amplitudes of the spectra with different delay times correctly. The amplitudes of the highly time-delayed experimental spectra are considerably smaller than expected from the theoretical model assuming a pure Maxwellian velocity distribution. We observed this effect at all investigated nozzle temperatures.

According to [15] and [16], a modification of the pure Maxwellian velocity distribution occurs, which depends on the Knudsen number K defined as

$$K:=\frac{\bar{\lambda}}{L_n}, \tag{12}$$

where $\bar{\lambda}$ is the mean free path of the atoms in the nozzle and L_n the length of the nozzle. For Knudsen numbers $K<10$ a deviation from the pure Maxwellian shape is predicted. This is caused by collisions inside the nozzle leading to a reduction of the number of slow atoms in the atomic beam. This effect is known as Zacharias effect [17]. For long nozzles with radius r_n and $L_n/r_n \gg 1$ (here $L_n/r_n \simeq 20$), the Zacharias effect can be expressed with the help of the function $P(K,x)$ leading to the corrected flux $f_c(x=v/v_0)$:

$$f_c(x)=f(x)P(K,x), \tag{13}$$

with

$$P(K,x)=\frac{\sqrt{\pi}\ \mathrm{erf}[g(x)]}{2g(x)},$$

$$g(x)=\sqrt{\frac{x^{-2/5}Fa_0(6,x)}{2^{3/2}K}}.$$

Here, the $v_r^{-2/5}$ dependence of the total scattering cross section on the relative velocity v_r of colliding particles at typical energies is accounted for. A table with values of the function $Fa_0(6,x)$ is given in Ref. [16]. For $K>10$ the corrected distribution $f_c(x)$ converges to a pure Maxwellian distribution since then collisions inside the nozzle become very unlikely. For $K<10$ the effect of collisions leads to a shift of $f_c(x)$ to higher relative velocities. This effect can be seen in Fig. 6, where the velocity distribution of flux is shown as it results from the fit of the time-resolved spectrum of Fig. 2. During the fit procedure the Knudsen number and the temperature of the atomic beam were free parameters. The temperature measured at the nozzle was 70.2 K. The best fit gives a temperature of 71.2 K, in fairly good agreement with the measured value. In this case of a relatively high temperature, the Knudsen number has been set to 0.05 corresponding to a mean free path inside the nozzle of 0.5 mm. The shifting effect on the modified velocity distribution is clearly visible.

For our high-precision measurements we usually cool the nozzle further down to temperatures around 7 K. At such low temperatures a considerable fraction of nondissociated molecular hydrogen in the atomic beam freezes to the walls of the nozzle, which leads to fewer collisions inside the nozzle. On the other hand, the pressure of background gas decreases

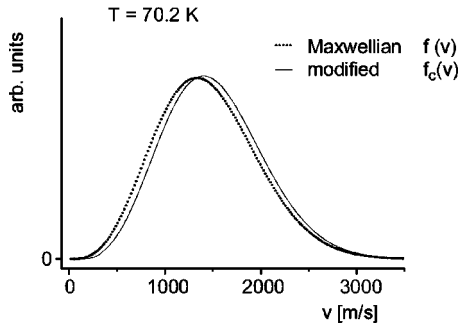

FIG. 6. Modified velocity distribution of the flux $f_c(v)$ as determined during the fit of the theoretical line shape to the experimental data as shown in Fig. 2. There is a deficiency of slow atoms in the beam due to collisions inside the nozzle.

from 10^{-5} to about 10^{-6} mbar due to the additional pumping of the cold surfaces. Thus at lower temperatures, a considerably higher flux of slow atoms will reach the detector. This effect is shown in Fig. 7 where the signals with delay times of 0 and 200 μs are shown for different temperatures of the nozzle. For temperatures below 10 K, signals with a delay time up to 2000 μs can be recorded with drastically reduced velocity-dependent systematic effects. Figure 8 shows a time-resolved spectrum recorded at a nozzle temperature of 7.4 K.

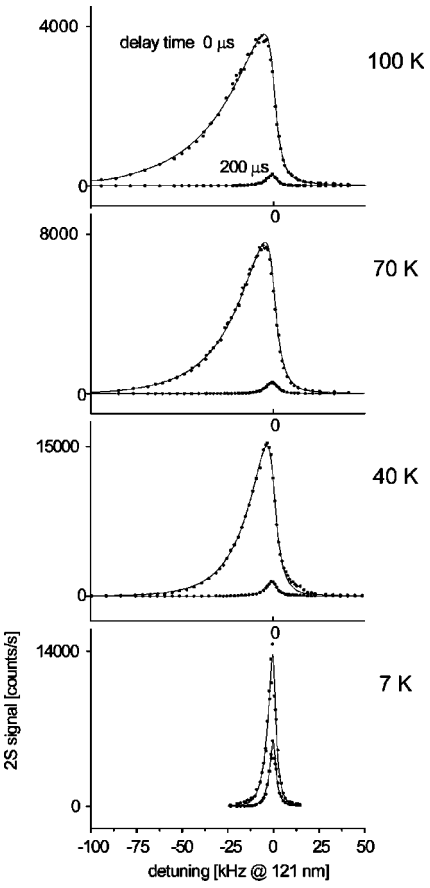

FIG. 7. Comparison of the signals with delay times of 0 and 200 μs for different temperatures of the nozzle. At temperatures below 10 K the flux of slow atoms increases substantially. The solid line is the theoretical line-shape model fitted to the data.

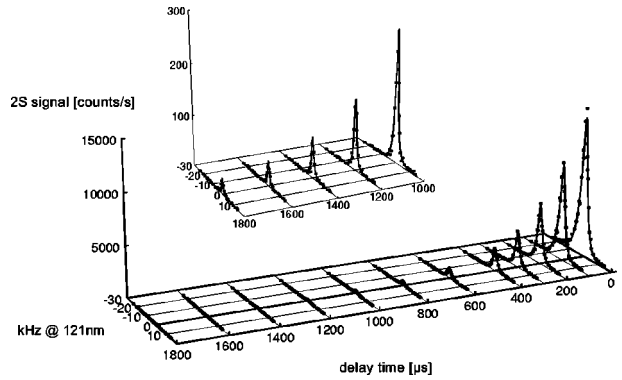

FIG. 8. Time-resolved $1S$-$2S$ spectrum in atomic hydrogen, recorded at a nozzle temperature of 7.4 K. The solid line is the theoretical line-shape model fitted to the experimental data. In the upper part, the five spectra with highest delay times are shown with a magnified scale. The corresponding atomic velocity distribution of the flux is shown in Fig. 9.

For temperatures of the nozzle ranging between 7 K and 100 K, all time-resolved spectra can be fit using a set of seven fit parameters with good agreement between the calculated and experimental spectra, as shown in Fig. 7. Besides the amplitude A, the temperature T of the atomic beam, the relative detuning Δ_{det}, and the Knudsen number K, three further fitting parameters are necessary. First, the theoretical spectra must be convolved with a Lorentzian profile of linewidth Γ_{Lor} to account for broadening effects in the experimental spectra that have not been incorporated in the calculation and that will be discussed later. Moreover, two additional parameters are needed to further modify the velocity distribution to describe an additional supression of very slow atoms. We ascribe this loss rate to collisions with the background gas, which preferably reduce the number of slow atoms reaching the detector [18]. We have modeled this suppression empirically by introducing two parameters v_s and v_{exp} as follows. Below the velocity v_s the exponent in $f(v)$ is chosen as $v^{v_{exp}}$ instead of v^3. Values for v_{exp} between 4 and 5 give good agreement for the amplitudes of the highly time-delayed spectra. Reference [18] gives an analytical expression for the probability $P(v)$ that an atom of the atomic beam with velocity v passes the interaction region and reaches the detector without colliding with a background gas particle. In our case the background gas mainly consists of molecular hydrogen, helium, and nitrogen, as measured with a mass spectrometer. To obtain the function $P(v)$ for our atomic beam experiment we calculated the total cross sections according to Refs. [19–21] for typical collisional energies between beam and background particles. For a temperature of the background gas of 250 K and a pressure of 10^{-6} mbar, a suppression of the signal of slow atoms is predicted in a similar way as modeled by the two empirically introduced parameters v_s and v_{exp}. We incorporated this analytical model of collisions in our line-shape model by taking the pressure of the background gas as a fit parameter instead of the two empirical parameters. It turned out that the χ^2 yielded in a fit is about a factor of 2 worse indicating that the analytical model does not describe the atomic beam properties the same way. This is probably due to the fact that for small collisional energies the total cross section strongly de-

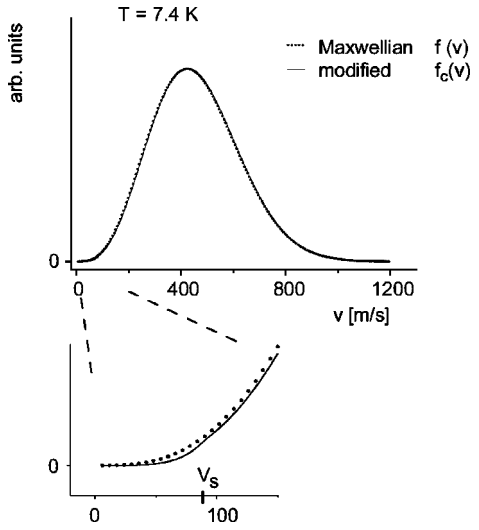

FIG. 9. Modified velocity distribution $f_c(v)$ corresponding to the time-resolved spectrum shown in Fig. 8. The slight shift to higher velocities with respect to the pure Maxwellian distribution $f(v)$ is due to collisions inside the nozzle. In the lower part, an additional modification of the distribution is visible. This effect is caused by collisions with the background gas, which further decrease the number of very slow atoms. The dotted line indicates a pure Maxwellian velocity distribution of the flux at the same temperature.

pends on the relative velocity whereas in $P(v)$ the effect of the background is averaged and described by the behavior of particles at the most probable velocity. Moreover, a velocity-dependent collisional quenching effect of excited hydrogen atoms is not accounted for in $P(v)$. Given the better fitting results of the empirical model and the simplifications necessary for the analytical model, we have decided to presently proceed with the empirical model.

Figure 9 shows the velocity distribution of the flux corresponding to the spectrum shown in Fig. 8. Here the Zacharias effect is quite small since molecular hydrogen freezes to the nozzle walls leading to a more dilute atomic beam. Below $v_s \simeq 90$ m/s, an exponent of $v_{exp}=4.7$ instead of 3 in the velocity distribution gives a good agreement with the signal strength of the observed experimental spectra. The temperature of the nozzle was measured to be 7.4 K. The fitting procedure gives a temperature of 7.2 K and a Knudsen number of 2.4. The additional modification for velocities below v_s is essential to describe the amplitudes of the highly time-delayed spectra correctly. This shows how sensitive the experiment is to small changes in the velocity distribution. Therefore, this line shape model is an interesting tool to study the gas kinetic properties of our atomic beam with very high sensitivity.

From the fit parameter Δ_{det} the unshifted center frequency of the spectra, corrected for the second-order Doppler effect, can be determined. Figure 10 shows the second-order Doppler shift of the spectrum at 7.4 K for different delay times. The points with error bars give the position of the line centers as found by fitting Lorentzian profiles to the time-resolved spectrum of Fig. 8. For comparison, the solid line represents the spline-interpolated position of the peak of the theoretical spectra. For small delay times the experimental line shape significantly deviates from a pure Lorentzian line

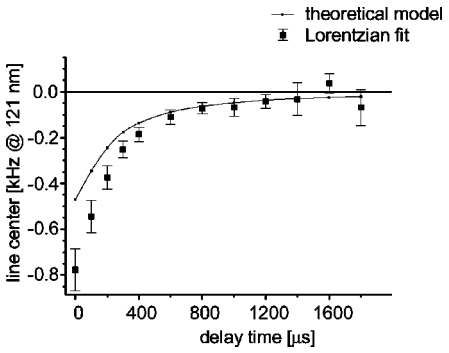

FIG. 10. Line centers as given by the theoretical model fit to the spectra of Fig. 8. The shift relative to the asymptote is due to the relativistic Doppler effect. The points with error bars are the line centers resulting from Lorentzian fits to the single spectra.

shape leading to the difference in the result between the two methods. As can be seen in Fig. 10 the relativistic Doppler shift of the individual spectra converges asymptotically towards zero with increasing delay time due to the decrease in velocity of the contributing atoms. For delay times higher than 800 μs fitting the line-shape model gives a result compatible with that obtained by fitting Lorentzians but with much better statistics. In fact, with this method the line center of a time-resolved hydrogen spectrum can be determined to an accuracy of about 1/100 of the linewidth since information from all individual spectra enters such a fit, the remaining uncertainty being only about 20 Hz at 121 nm. At this point, we wish to stress that the quantity Δ_{det} is very robust with respect to the values of the other fit parameters. While it is not possible to extrapolate the line centers from Lorentzian fits with high accuracy due to the poor statistics of the highly time-delayed spectra, the presented method allows a very accurate determination of the transition frequency.

Note that in the evaluation of the expression in Eq. (9), only a full integration over the entire orifice of the nozzle leads to a good agreement between the model and the experimental data. We assume the starting points of the trajectories to be equally distributed over the orifice of the nozzle. Alternatively, we calculated a set of theoretical data assuming that all atomic trajectories start from the nozzle walls. As it turned out, this approach leads to a poor agreement and to unphysical values for the fitted temperature of the atomic beam, being typically only about half as large as the value of the measured temperature. As discussed previously, the Knudsen number given in our experiment implies that collisions in the nozzle are expected to influence the properties of the beam. According to [15] a nozzle is called transparent if $K \gg 1$. Then the properties of the atomic beam are solely determined by collisions with the walls of the nozzle. For smaller Knudsen numbers, as in our case, the flux is called viscous. The magnitude of the Knudsen numbers as determined for our nozzle are consistent with the assumption that atomic trajectories start from the whole orifice of the nozzle and not only from the walls. A more detailed discussion of this aspect is given in [22].

IV. SYSTEMATIC EFFECTS AND TOTAL UNCERTAINTY

In this section we give a short overview of known systematic effects that are important for the 1S-2S transition at

the present level of accuracy. All frequencies are given at 121 nm. In two-photon excitation the first-order Doppler shift cancels. The second-order Doppler effect redshifts the transition frequency. The shift strongly depends on the temperature of the atomic beam. As demonstrated in the previous section, the Doppler shift can be corrected with a remaining uncertainty of about 20 Hz at 121 nm by fitting our theoretical line-shape model to a time-resolved spectrum recorded at temperatures below 10 K.

The ac-Stark shift blueshifts the transition frequency linearly with the intensity of the excitation light field: $\Delta\nu_{ac\text{-}Stark}=2I\beta_{ac\text{-}Stark}$ and $\beta_{ac\text{-}Stark}=1.667\times10^{-4}$ Hz $(\mathrm{W/m^2})^{-1}$ [23], where I is the intensity in each direction in the enhancement resonator. We can record time-resolved spectra with a good signal-to-noise ratio at light powers of only 20 mW in each direction to keep the ac-Stark shift small, although more UV power is available. Taking into account the beam size and averaging numerically over all trajectories through the standing wave light field yields a corresponding ac-Stark shift of about 50 Hz. Even if this shift is poorly compensated by measuring at different light powers and extrapolating, the total uncertainty can be kept below values of about 20 Hz.

Static electric fields E mix the $2S$ and the nearby $2P$ state. The dc-Stark effect shifts the transition frequency by an amount of $\Delta\nu_{dc\text{-}Stark}=+3600E^2$ Hz $(\mathrm{V/cm})^{-2}$ [24]. Therefore, the interaction region in our setup is surrounded by a graphite-coated Faraday cage to avoid static charges and to keep an atom on the same electrical potential along its way from the nozzle to the detector. Fields below 30 mV/cm have been measured [14] by Biraben and co-workers using a similar apparatus. The effect on the $1S$-$2S$ transition frequency thus is just a few Hz.

The pressure shift of the $1S$-$2S$ transition was experimentally measured in a hydrogen gas cell to be $\Delta\nu_p=8.4$ MHz/mbar [25]. A slightly smaller coefficient of the pressure shift is given in [3]. At nozzle temperatures below 10 K, the pressure in our vacuum chamber is about 10^{-6} mbar, resulting in a pressure shift of less than 10 Hz.

For the case of two-photon spectroscopy in an ideal standing wave, the wave vectors of counterpropagating photons are oriented exactly anticollinearly with respect to each other. Nevertheless, in a collimated optical standing wave, the transverse localization of the photons leads to an uncertainty $\Delta\mathbf{k}$ in the orientation of the wave vectors $\mathbf{k}$. Therefore, two absorbed photons may not propagate exactly anticollinear. In first order a term $\Delta\mathbf{k}\,\mathbf{v}$ appears, corresponding to the well-known time-of-flight broadening that is already included in the calculations. In second order a recoil shift of order $\Delta\mathbf{k}^2/2M$ remains that is not yet included but contributes less than 10 Hz with the experimentally realized beam-waist of 230 μm [26]. An admixture of higher-order modes in the optical resonator due to imperfect adjustment may lead to a remaining first-order Doppler shift. The resulting shift has been estimated in [22] to be below some few Hz. Further, we want to point out that no shift due to the geometrical phase of the standing wave field occurs, since the two photons are absorbed instantaneously, i.e., at the same position in the case of two-photon excitation.

Taking into account all these systematic effects, it is possible to determine the unperturbed hydrogen $1S$-$2S$ transition frequency from the time-resolved spectra with a remaining uncertainty of about 40 Hz, corresponding to an accuracy of about 1.5×10^{-14}. The total measurement time necessary to record a typical time-resolved spectrum is on the order of 100 s. The good agreement between the theoretical line-shape model and the experimental spectra indicates that the major systematic effects are well understood. To date, the accuracy of our last absolute frequency measurement [1] is limited to 3.3×10^{-13} by the reproducibility of the secondary He-Ne frequency standard, which we use as an intermediate reference for our phase-coherent frequency chain. Therefore, in our recent measurements of the $1S$-$2S$ absolute frequency and the hydrogen-deuterium isotope shift of this transition, it was sufficient to fit Lorentzian profiles to the time-delayed experimental spectra to determine the center frequency.

An important feature of the time-delayed measurement technique could be investigated with the help of our line-shape model. While the simple calculation of the maximum velocity $v_{max}=d/\tau$ just sets an upper limit to the velocity of atoms contributing to a signal with delay time τ, a closer examination reveals that in fact the main contribution is due to atoms at velocities around $v_{max}/2$, which results in a relativistic Doppler shift four times smaller than roughly estimated [22]. This is due to the fact that atoms close to v_{max} interact for too short a time with the light field and thus just give a minor contribution to the signal.

It is also interesting to look at the major effects that cause the width of the experimental $1S$-$2S$ spectra to considerably exceed the natural linewidth. The line-shape model predicts time-of-flight broadening and broadening arising from the different second-order Doppler shifts of the different velocity classes in the atomic beam. Stray electric fields may cause a broadening of spectra via the reduction of the lifetime. We apply a static magnetic field to separate the field-sensitive component of the $1S$-$2S$ transition ($F=1\rightarrow1, m_F=0\rightarrow0$) to excite only the $1S$-$2S$($F=1\rightarrow1, m_F=\pm1\rightarrow\pm1$) transitions. The $m_F=-1\rightarrow-1$ and the $m_F=+1\rightarrow+1$ transitions are split by about 72 Hz/G due to a small relativistic difference in the electron g factors of the $1S$ and $2S$ state [7]. With an applied magnetic field of about 3 G, this splitting is too small to be observed in our strongly time-of-flight broadened spectra. Nevertheless, the splitting of about 200 Hz acts like an additional broadening effect and may be included in the additional 1 or 2 kHz Lorentzian linewidth Γ_{Lor} with which the theoretical spectra must be convolved to achieve good agreement with the width of the experimental spectra. The absorption of a further photon at 243 nm is sufficient to ionize an atom from the $2S$ state to continuum. This effect increases the linewidth by $\Delta\nu_{Ioni}=2I\beta_{Ioni}$ where $\beta_{Ioni}=1.803\times10^{-4}$ Hz $(\mathrm{W/m^2})^{-1}$ [23]. Again, I is the intensity in each direction in the enhancement resonator. With the help of our line-shape model we have calculated a net broadening of 3.5(8) Hz/mW for our excitation geometry. For high light powers on the order of 100 mW, this additional broadening is observable in the spectra at the present level of resolution.

Since the additional linewidth can be partially ascribed to the above discussed effects, we do not believe that only the linewidth of our dye laser system limits the spectral resolution of the $1S$-$2S$ spectra. Nevertheless, from the typical value $\Gamma_{Lor}=1.2$ kHz at 121 nm, an upper limit of roughly

300 Hz at 486 nm for the linewidth of the dye laser can be derived.

V. CONCLUSIONS

We have presented a theoretical line-shape model that is in good agreement with our experimentally observed hydrogen $1S$-$2S$ spectra and allows us to fully exploit the spectral resolution that can be achieved with our time-resolved measurement scheme. We now can determine the $1S$-$2S$ transition frequency from the experimental spectra within 1.5×10^{-14}. The Q factor we have achieved in spectroscopy of the hydrogen $1S$-$2S$ transition is the highest in any neutral atom. In the future, we plan to further improve the frequency uncertainty by using laser-cooled hydrogen atoms [27]. The hydrogen $1S$-$2S$ transition is a promising candidate for an optical clock. Moreover, this atom, being accessible for precise calculations of its transition frequencies, allows both the test of basic physical theories as well as the determination of fundamental constants.

ACKNOWLEDGMENTS

We are grateful to C. J. Bordé and C. Zimmermann for many helpful discussions. We thank P. V. Storm and M. Niering for carefully reading the manuscript.

[1] Th. Udem, A. Huber, B. Gross, J. Reichert, M. Prevedelli, M. Weitz, and T. W. Hänsch, Phys. Rev. Lett. **79**, 2646 (1997).
[2] B. de Beauvoir, F. Nez, L. Julien, B. Cagnac, F. Biraben, D. Touahri, L. Hilico, O. Acef, A. Clairon, and J. J. Zondy, Phys. Rev. Lett. **78**, 440 (1997).
[3] D. J. Berkeland, E. A. Hinds, and M. G. Boshier, Phys. Rev. Lett. **75**, 2470 (1995).
[4] A. Huber, Th. Udem, B. Gross, J. Reichert, M. Kourogi, K. Pachucki, M. Weitz, and T. W. Hänsch, Phys. Rev. Lett. **80**, 468 (1998).
[5] D. G. Fried, Th. C. Killian, L. Willmann, D. Landhuis, S. C. Moss, D. Kleppner, and Th. J. Greytak, Phys. Rev. Lett. **81**, 3811 (1998).
[6] Recommendation 1 (CI–1997) adopted by the Comité International des Poids et Mesures (CIPM) at its 86th meeting in 1997 [Metrologia (to be published)].
[7] F. Schmidt-Kaler, D. Leibfried, S. Seel, C. Zimmermann, W. König, M. Weitz, and T. W. Hänsch, Phys. Rev. A **51**, 2789 (1995).
[8] C. Cohen-Tannoudji, B. Diu, and F. Laloë, *Quantum Mechanics* (Wiley, New York, 1977), Vol. I.
[9] P. Meystre and M. Sargent, *Elements of Quantum Optics* (Springer, Berlin, 1989).
[10] C. J. Bordé, in *Advances in Laser Spectroscopy*, edited by F. T. Arecchi, F. Strumia, and H. Walther (Plenum, New York, 1983).
[11] F. Bassani, J. J. Forney, and A. Quattropani, Phys. Rev. Lett. **39**, 1070 (1977).
[12] H. Kogelnik and T. Li, Appl. Opt. **5**, 1550 (1966).
[13] W. H. Press, B. P. Flannery, S. A. Teukolsky, and W. T. Vetterling, *Numerical Recipes in Pascal* (Cambridge University Press, Cambridge, 1989).
[14] J. C. Garreau, M. Allegrini, L. Julien, and F. Biraben, J. Phys. (France) **51**, 2263 (1990); **51**, 2275 (1990); **51**, 2293 (1990).
[15] G. Scoles, D. Bassi, U. Buck, and D. Laine, *Atomic and Molecular Beam Methods* (Oxford University Press, New York, 1988), Vol. I.
[16] K. Berkling, R. Helbing, K. Kramer, H. Pauly, Ch. Schlier, and P. Toschek, Z. Phys. **166**, 406 (1962).
[17] N. F. Ramsey, Rev. Mod. Phys. **62**, 541 (1990).
[18] N. F. Ramsey, *Molecular Beams*, 2nd ed. (Clarendon, Oxford, 1989).
[19] E. Gislason and M. Sizun, J. Chem. Phys. **93**, 2469 (1990).
[20] R. Gengenbach, Ch. Hahn, and J. P. Toennies, J. Chem. Phys. **62**, 3620 (1975).
[21] S. P. Walch, J. Chem. Phys. **93**, 2384 (1990).
[22] A. Huber, Ph.D. thesis, LMU-München, 1997.
[23] R. G. Beausoleil, Ph.D. thesis, Stanford University, 1986.
[24] H. A. Bethe and E. E. Salpeter, *Quantum Mechanics of One- and Two-Electron Atoms* (Plenum, New York, 1977).
[25] D. H. McIntyre, R. G. Beausoleil, C. J. Foot, E. A. Hildum, B. Coulliaud, and T. W. Hänsch, Phys. Rev. A **39**, 4591 (1989).
[26] C. J. Bordé *et al.* (private communication).
[27] J. Walz and K. Eikema (private communication).